Heliyon

Received:
11 August 2018
Revised:
28 January 2019
Accepted:
12 April 2019

Cite as: Ghasem Sargazi, Daryoush Afzali, Ali Mostafavi, Alireza Shadman, Babak Rezaee, Payam Zarrintaj, Mohammad Reza Saeb, Seeram Ramakrishna, Masoud Mozafari. Chitosan/polyvinyl alcohol nanofibrous membranes: towards green super-adsorbents for toxic gases.
Heliyon 5 (2019) e01527.
doi: 10.1016/j.heliyon.2019.e01527

Chitosan/polyvinyl alcohol nanofibrous membranes: towards green super-adsorbents for toxic gases

Ghasem Sargazi [a], Daryoush Afzali [b], Ali Mostafavi [a], Alireza Shadman [c], Babak Rezaee [c], Payam Zarrintaj [d,e,f], Mohammad Reza Saeb [g,*], Seeram Ramakrishna [h], Masoud Mozafari [i,j,k,*]

[a] *Department of Nanotechnology Engineering, Mineral Industries Research Center, Shahid Bahonar University of Kerman, Kerman, Iran*

[b] *Department of Chemistry, Graduate University of Advanced Technology, Kerman, Iran*

[c] *Department of Chemistry, Faculty of Science, Shahid Bahonar University of Kerman, Kerman, Iran*

[d] *Polymer Engineering Department, Faculty of Engineering, Urmia University, Urmia, Iran*

[e] *Color and Polymer Research Center (CPRC), Amirkabir University of Technology, P.O. Box 15875-4413, Tehran, Iran*

[f] *Advanced Materials Group, Iranian Color Society (ICS), Tehran, Iran*

[g] *Department of Resin and Additive, Institute for Color Science and Technology, Tehran, Iran*

[h] *Center for Nanofibers & Nanotechnology, Department of Mechanical Engineering, National University of Singapore, Singapore*

[i] *Bioengineering Research Group, Nanotechnology and Advanced Materials Department, Materials and Energy Research Center (MERC), Tehran, Iran*

[j] *Cellular and Molecular Research Center, Iran University of Medical Sciences, Tehran, Iran*

[k] *Department of Tissue Engineering & Regenerative Medicine, Faculty of Advanced Technologies in Medicine, Iran University of Medical Sciences, Tehran, Iran*

[*] Corresponding authors.
E-mail addresses: saeb-mr@icrc.ac.ir (M.R. Saeb), mozafari.masoud@gmail.com (M. Mozafari).

Abstract

Removal of hazardous gases from the atmosphere has become a big challenge for scientists and engineers alike. Eco-friendly nature of biopolymers has given a new dimension to the debate within the environmental science area but attempts mainly

https://doi.org/10.1016/j.heliyon.2019.e01527

failed to cleanse the air stream of toxic gases as a consequence of design imperfections. In this work, green electrospun nanofibrous membranes based on chitosan (Cs)/polyvinyl alcohol (PVA) composite with a very high carbon monoxide adsorption capacity (much higher than the values one may expect from activated carbon and zeolite adsorbents, and also higher than that of the metal-organic framework) are developed. 2^{k-1} factorial design, response surface and desirability function analyses are merged to optimize the electrospinning parameters for functional-based carbon monoxide elimination. The best Cs/PVA adsorbent obtained through multi-objective optimization has a very high desirability value level of 0.953. Optimized electrospinning parameters are: Voltage = 17 kV, spinning distance = 13 cm, flow rate = 0.2 mL/h, and PVA concentration = 6 wt.%; and optimized properties are: maximum thermal stability = 329 °C, minimum fiber diameter = 9.8 nm, and maximum surface area = 2204 m^2/g. This work opens a new era for taking the next steps towards the design and optimization of green super-adsorbents for gaseous contaminations.

Keyword: Materials science

1. Introduction

The ongoing concerns about environmental threats underline the need for developing innovative eco-friendly strategies for the sake of a cleaner planet. Material design plays a key role in achieving a promising level of environment protection, where polymers appear as the building blocks of complex materials and systems responsible for the strong *Will* to *Live* [1, 2, 3]. Meanwhile, polymer recycling has remained as the main challenge for technologists that always are seeking green plans. Human beings are forewarned that the aerial footage caused by polymer disposal is a big threat to the environment. This may need continued supervision and perceived limitations against the uncontrolled use of polymers, but polymer scientists in a parallel manner attempt to soldier on with biodegradable polymers to answer vexed questions [4, 5, 6]. Moreover, they have little by little learned how to harmonize the contradiction between good biodegradability and poor mechanical properties of green polymers.

Polysaccharides are biodegradable carbohydrates gained from nature among which are agarose, alginate, starch and gelatin, together with chitosan (Cs) which appears on the top of the game thanks to its amine-rich reactive structure [7, 8, 9, 10]. According to the statistics, research on chitosan is becoming progressively widespread (Fig. 1A). Cs has attracted too much attention in the fabrication of scaffolds for tissue engineering [11, 12, 13]. But, its poor mechanical properties necessitate the need to use a synthetic biodegradable polymer as a supplement. Polyvinyl alcohol (PVA) is a synthetic biodegradable polymer that received much attention in recent years

https://doi.org/10.1016/j.heliyon.2019.e01527

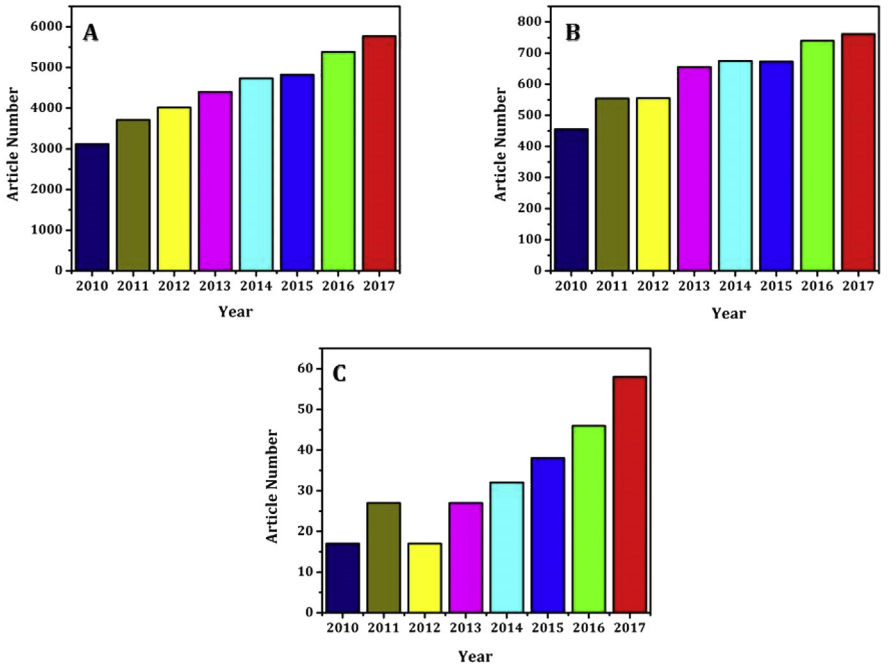

Fig. 1. The number of recent research articles during 2010−2017 on chitosan (A), PVA (B), Cs/PVA (C) (According to Scopus).

(Fig. 1B) [14]. In this sense, it has entered the game to play the role of mechanical property supplement to Cs [15, 16, 17]. Research on Cs/PVA is becoming more important, as featured by a four-fold increase in the number of publication in this field in between 2010 and 2017 (Fig. 1C) [18, 19, 20]. The Cs/PVA composites have been mainly utilized in regenerative medicine [21, 22, 23], but not practised in removal of hazardous contaminants like carbon monoxide from air stream.

It was reported that the PVA/CS along with zinc oxide was utilized for dye removal. ZnO addition caused to red shifting and intensities. Moreover, PVA/CS nanofibers biocompatibility was assessed using NIH3T3 cells which was revealed that PVA/CS nanofibers biocompatibility was improved in comparison with pristine PVA [24]. PVA/CS modified with aminated Fe3O4 was used to remove the Cr(VI) and Pb(II) ions which pseudo-first-order kinetic and Langmuir isotherm models were utilized to describe the kinetic model [25]. Moreover, lead(II) and cadmium(II) ions removal from wastewater was studied using PVA/CS nanofibers. It was shown that the Langmuir isotherm was the appropriate model for adsorption. Other metal ions did not affect the Pb(II) and Cd(II) ions which such ions adsorbed more than 94% [26].

The earth suffers from various kinds of pollutions, but air pollution hazard posed by carbon monoxide (CO) is the most dangerous ones to the human beings, plants, animals, and ecosystem [27, 28, 29]. Zeolites and metal-organic frameworks have been

https://doi.org/10.1016/j.heliyon.2019.e01527

frequently applied in CO adsorption due to their high surface area and high porosity, but their low biocompatibility and biodegradability is a big challenge from the environmental perspective [30, 31, 32, 33]. Biocompatible nanofibrous polymers rely on either eco-friendly or biological features for such purposes [34, 35]. Electrospinning is a facile method for fabricating nanofibers for CO removal with a wide range of diameter; however, to achieve a functional performance nanofiber size must be optimized [36, 37, 38]. There was a paradigm shift from Edisonian to purposeful experimental design approaches to enhance system performance [17, 39, 40, 41, 42]. Response surface methodology (RSM) is a combination of mathematical and statistical routes utilized for modeling, optimization, and interpreting the influence of system variables on desired targets [43, 44, 45]. It contains three phases: (i) identifying the most influential factors by screening them from process variables; (ii) performing experiments to find control factors and their variation intervals to recognize the first response surface in the region of optimum; and (iii) positioning into the optimal region by fitting the best interpolating function to experimental data by choosing a design model [46, 47].

Chitosan (Cs) is derived from chitin as a basic element of D- glucosamine and can be extracted successfully from shellfish [48, 49]. In this work, green PVA/Cs electrospun nanofibrous membranes are designed and their properties including thermal stability, surface area, and size distribution are optimized using multiobjective optimization based on response surface and desirability function analyses. First, a series of Cs/PVA nanofibers containing various amounts of PVA are prepared and fully characterized for morphology, thermal stability, textural and CO removal capacity were prepared based on 2^{k-1} factorial design, then RSM and desirability function were applied to optimize their properties by fine tuning the process and material parameters including spinning voltage, spinning distance, flow rate, and PVA concentration. Optimizing large number of factors to achieve the proper nanofibers necessitates large number of experiments which consume lots of energy and cost, in this regards, experimental design has been used to reduce such remedies. However, full factorial design is a too expensive method; on the other hand, fractional factorial design is a cost-effective and applicable method in which 2k-p! design analysing k factors with only 2k-p experiments is required (e.g. 2^{k-1} and 2^{k-2} design requires only half and one quarter of the experiments as many experiments, respectively).

In this work, for the first time PVA/CS nanofibers was utilized for CO removal from air stream with optimized condition which were derived using fractional factorial design and compared with other adsorbents. Such study paves a way for future investigation on toxic gas adsorption which can be potentially used as cost-effective air purification filters.

https://doi.org/10.1016/j.heliyon.2019.e01527

2. Experimental

2.1. Material and instrument

All the chemicals including PVA powder (Mw: 85,000−124,000, 96%, Merck), Cs powder (Mw: 500−1000, 99%, Aldrich), and acetic acid (99%, Aldrich) were used without further purification. The Cs/PVA composite nanofibers were characterized by a variety of techniques including scanning electron microscopy (SEM), Fourier-transform infrared spectroscopy (FTIR), BET surface area, thermogravimetric analysis (TGA), and differential scanning calorimetry (DSC). For SEM analysis (Philips xl30), the fibrous samples were gold-sputtered with a thin layer of gold. The FTIR (SHIMADZU FT 8400 Spectrometer) was recorded on a spectrometer in the range of 500−4000 cm^{-1} using the KBr disk. Nitrogen adsorption technique (Belsorp mini II) was applied to determine pore textural properties including the specific surface area, pore volume, and pore diameter. TGA (SCINCO thermal gravimeter S-15000) and DSC (STA449F3, Netzsch) were carried out at the heating rate of 5° C/min from room temperature to 800°C under a dry N_2 atmosphere.

2.2. Synthesis of PVA/Cs-CNs

PVA/Cs solution (weight ratio of PVA:Cs was fixed at 65:15 in 5% acetic acid) was dissolved in acetic acid. The concentration of the PVA precursor was varied from 6 to 10 wt% and mixed under magnetic stirring for 1 h at 83 °C. The product, hereafter referred to as PVA/Cs-CNs, was fabricated by electrospinning method. In optimum conditions, the applied voltage was 17 kV and the electrospinning distance was 13 cm. The solutions were injected from the syringe pump with flow rates of 0.20 mL/h. Fig. 2 illustrates the schematic chart of PVA/Cs-CNs preparation.

2.3. 2^{k-1} factorial design

The 2^{k-1} fractional factorial design refers to the designs analysing k factors each having just two levels (−1, and +1), with half of the full factorial 2^k design's runs. By screening, one can refer to the process of screening a large number of factors that might be important in the experiment. Moreover, independent 2^{k-1} factorial design requires the observations randomly selected from the treatment population. In the 2^{k-1} factorial design, the systematic effects of different synthesis factors could be considered by implementing the analysis of variance (ANOVA) and a system could be investigated using RSM to optimize the experimental conditions. In fact, the use of this design could help one to find the best experimental condition and perform the targeted experiments with fewer repetitions [50, 51].

https://doi.org/10.1016/j.heliyon.2019.e01527

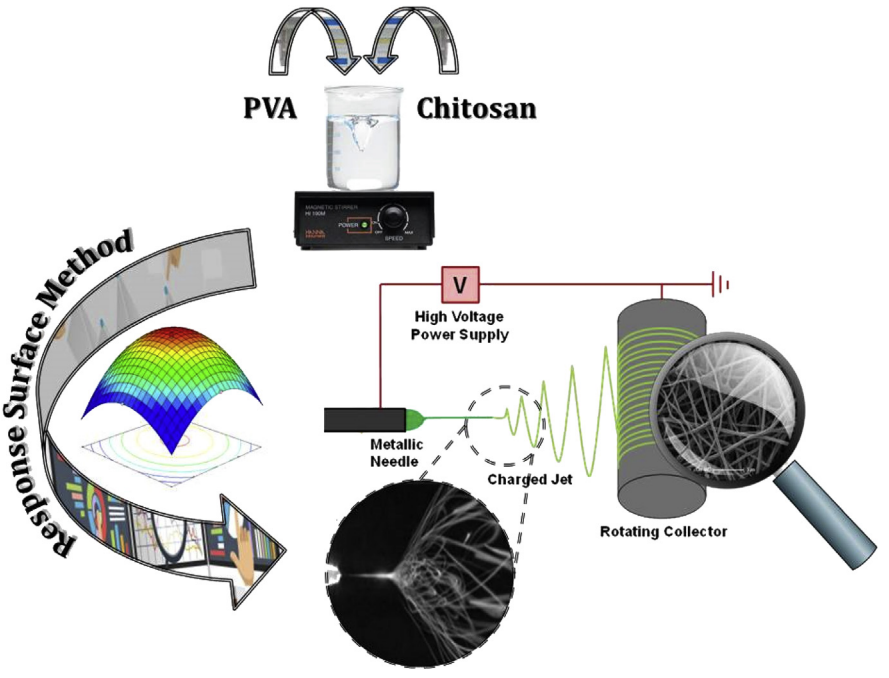

Fig. 2. Schematic of PVA/Cs-CNs preparation by electrospinning method.

2.4. Response surface methodology (RSM)

RSM is a technique for the process optimization, which enjoys from the benefits of statistics and mathematics. Using RSM plots, it is possible to optimize the main factors affecting electrospinning efficiency to achieve the most desirable percentage elongation. The response surface optimization was performed to determine the best synthesis parameter needed for production of desired nanofibers [52, 53]. Multi-objective optimization as performed using desirability function approach based on interpolating functions proposed by the RSM to find the best set of electrospinning parameters for optimized removal of green electrospun adsorbents with minimum size distribution, maximum thermal stability, and maximum surface area for carbon monoxide adsorption.

3. Results and discussion

3.1. Morphology and diameter adjustment

Fig. 3 shows the SEM micrograph of the PVA/Cs-CNs prepared from the precursors under optimum conditions (voltage: 17 kV, electrospinning distance: 13 cm, flow rate: 0.20 mL/h, and PVA concentration: 6 wt%). This micrograph reveals that PVA/Cs-CNs synthesized under optimum conditions have narrow size distribution (without beads) with the low diameter of about 10.7 nm through the fibrous matrix. On the other hand, SEM micrograph of the PVA/Cs-CNs in terms of uniform shape

https://doi.org/10.1016/j.heliyon.2019.e01527

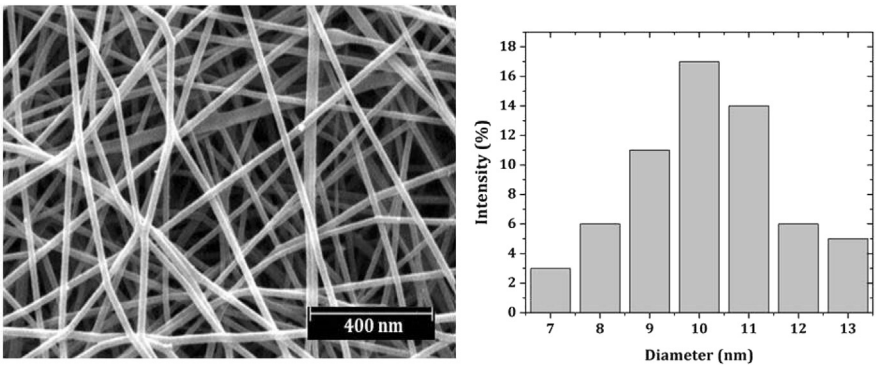

Fig. 3. SEM micrograph of the PVA/Cs-CNs synthesized with diameter dispersion.

was different from that of the previous research, which can be attributed to the effects of electrospinning conditions on the morphology of the final product [54].

3.2. FTIR characterization

FTIR spectra of the Cs and PVA powders and that of PVA/Cs-CNs are displayed in Fig. 4. The FT-IR spectrum of PVA powder shows absorption peaks near 3319, 2937, 1431, and 1007 cm^{-1}, which are related to OH, CH, CHOH, and CO groups, respectively [54]. Cs powder exhibits frequencies at 3427 and 3328 cm^{-1}, which are assigned to OH and NH bonds, respectively. The feature absorption peaks near 1656 and 1590 cm^{-1} are attributed to amide groups. Furthermore, the frequency at 1356 cm^{-1} is assigned to CO bond [55]. The FTIR spectrum of PVA/Cs-CNs shows peaks at 3384 and 3210 cm^{-1}, which are attributed to OH and NH stretching vibrations, respectively. Absorption bands near 2848, 1002, and 1592 cm^{-1} are also assigned to CH, CO, and amide groups, respectively. In conclusion, the PVA/Cs-CNs show the frequency bands related to PVA and Cs compounds [56].

3.3. Textural properties

PVA/Cs-CNs samples were washed with deionized water four times to eliminate impurities from the pores. Textural properties including specific surface area (i.e. 1920 m^2/g), pore diameter (i.e. 1.81 nm), and pore volume (i.e. 0.064 cm^3/g) of the PVA/Cs-CNs synthesized under optimum conditions of electrospinning were determined by N_2 adsorption at 77 K. Adsorption isotherms (Fig. 5) are obtained by measuring the amount of gas adsorbed across a wide range of relative pressures at the constant temperature (typically liquid N_2, 77 K) [57]. The adsorption isotherm of the Cs/PVA-CNs synthesized under optimum conditions of electrospinning process (Fig. 6) was similar to the first type that pores were typically microporous. Textural properties of the PVA/Cs-microporous polymer prepared in this work are different from a

https://doi.org/10.1016/j.heliyon.2019.e01527

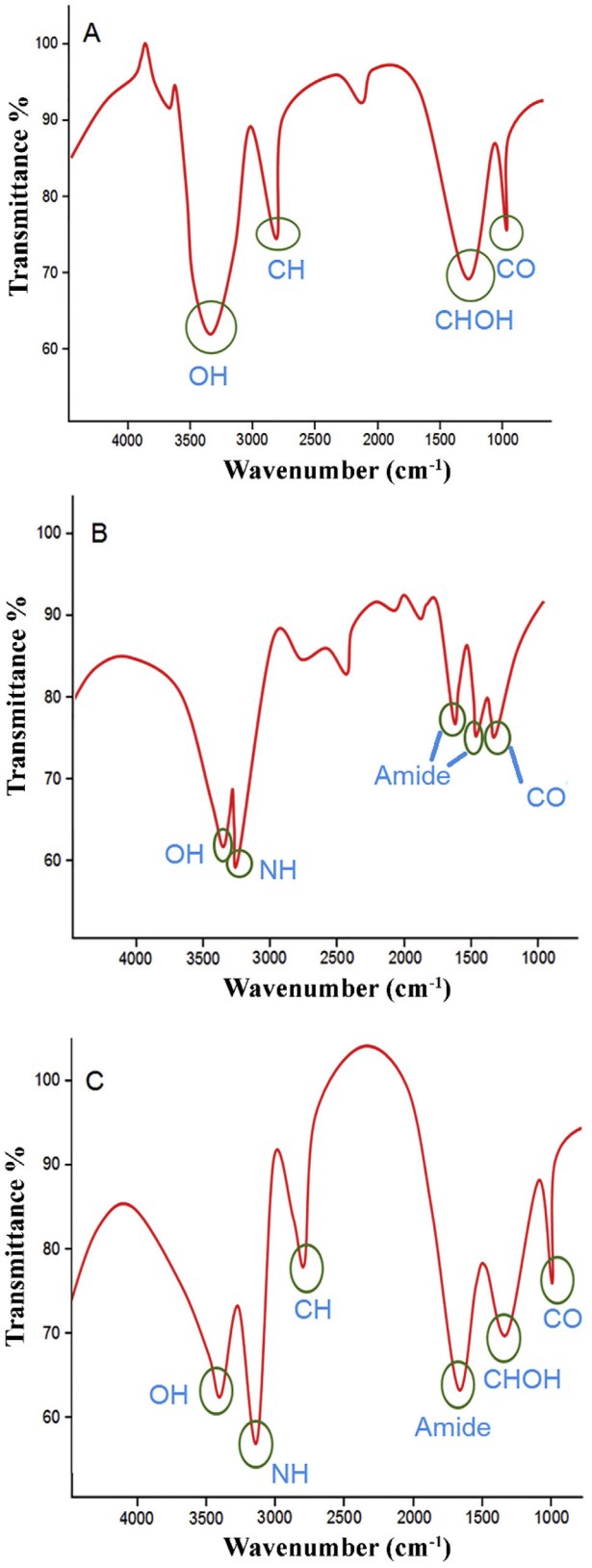

https://doi.org/10.1016/j.heliyon.2019.e01527

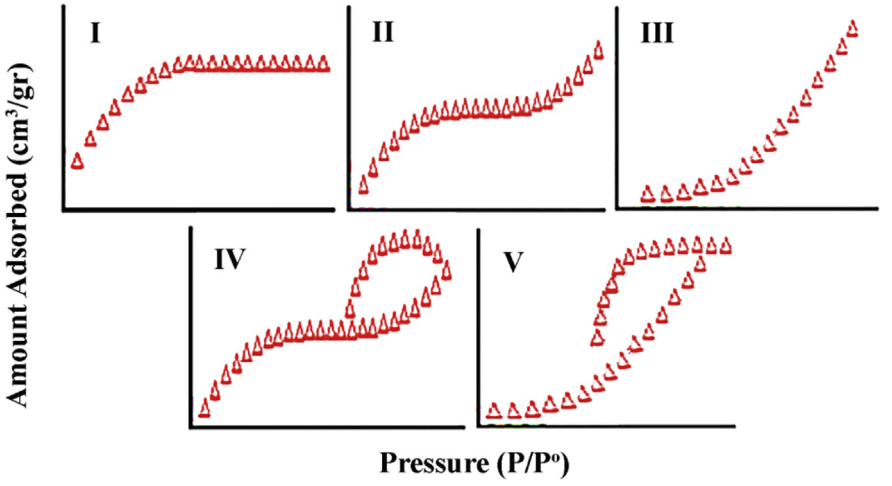

Fig. 5. Classical isotherm types described by Brunauer, Emmett, and Teller [57].

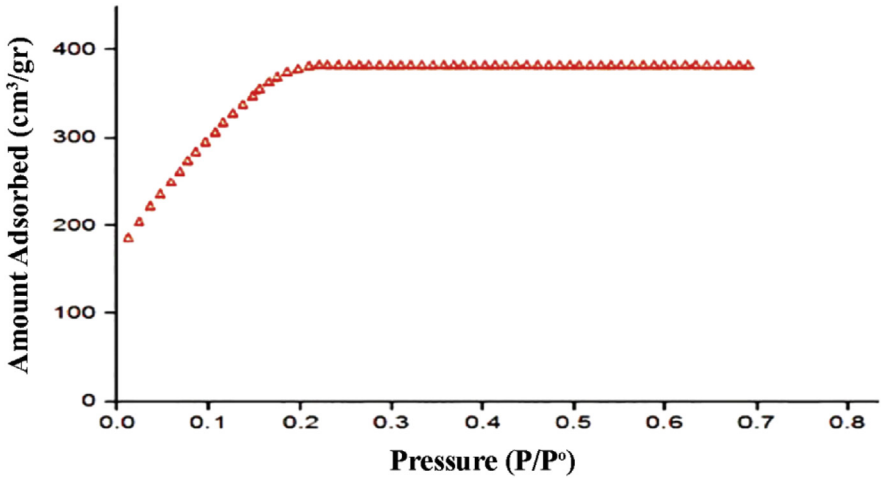

Fig. 6. Adsorption isotherm of the PVA/Cs-CNs synthesized under optimum conditions.

previous research performed on chitosan covalently crosslinked with poly(ethylene glycol) diacid as crosslinking agent in terms of the specific surface area and pore diameter, which may be related to the effects of electrospinning conditions on the textural properties of the final products in the presence of PVA [58].

Based on comparison between Figs. 5 and 6, it can be confer that the CO adsorption using PVA/CS nanofibers obeyed the Langmuir isotherm which was utilized as a proper homogeneous adsorption in case that the adsorbate molecules contains equal adsorption activation energy.

Fig. 4. FT-IR spectra of PVA powder (A), Cs powder (B), and PVA/Cs-CNs (C).

https://doi.org/10.1016/j.heliyon.2019.e01527

3.4. Thermal analysis

Fig. 7 shows the TGA curve of the electrospinning-assisted synthesized PVA/Cs-CNs in optimum conditions. It can be seen that the thermal behaviour of the product can be interpreted on the basis of three separate stages. The first stage is attributed to the vanishing of the adsorbed acetic acid (mass change: −9.61 %), in which the solvent is evaporated. In the second stage, the trapping solvent (mass change: −7.13 %) is evaporated. Large weight loss is due to the third stage in which disintegration of the structure is happened. The structural acetic acid, which has bonded to Cs atoms, is possible eliminated from the sample before 180 °C. As a supplement, Fig. 7 exhibits the DSC analysis of PVA/Cs-CNs in the right-hand axis, confirming that the decomposition behaviour of the compound can be divided into three distinguished stages. The first peak that appears at 120−130 °C can be related to the sample moisture and the latter peak at ~175 °C is attributed to the evaporation of trapped solvent. The significant weight loss at ~329 °C can be related to the pure sample decomposition, which means that the PVA/Cs-CNs have thermal stability up to ~320 °C [59, 60].

3.5. Experimental design

Once the structure of the electrospun PVA/Cs-CNs was evaluated, 2^{k-1} factorial design was carried out in the pilot to study the effects of electrospinning parameters on the PVA/Cs properties including size distribution (SD), surface area (SA), and thermal stability (TS). Four factors were voltage (A), spinning distance (B), flow rate (C), and PVA concentration (D) and each factor was present at two levels (Table 1). The design matrix and response data obtained from 2 replicates of the 8 experiments are presented in Table 2 (the 16 runs were made in a random order).

Fig. 8 exhibits that under different synthesis conditions, including different voltages, spinning distances, flow rates, and PVA concentrations, PVA/Cs-CNs had different diameter sizes and morphologies so that the sample ***E***

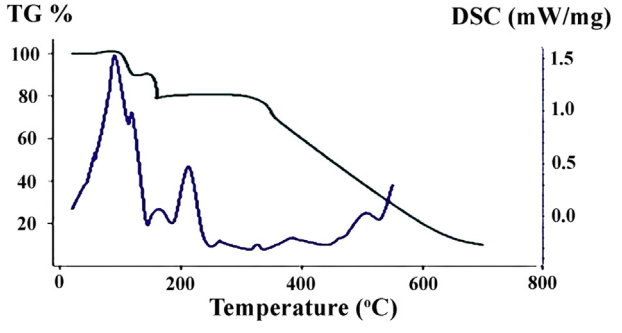

Fig. 7. TGA and DSC plots of electrospinning-assisted synthesized PVA/Cs-CNs.

https://doi.org/10.1016/j.heliyon.2019.e01527

Table 1. Coded levels and range of independent variables for 2^{k-1} factorial design.

Level	Coded level	Uncoded level			
		Voltage (kV)	Spinning distance (cm)	Flow rate (mL/h)	PVA concentration (wt.%)
High	+1	19	13	0.20	10
Low	−1	17	10	0.15	6
Coded Formula : $\frac{\mathbf{x} - \frac{\mathbf{x}(\mathbf{high}) + \mathbf{x}(\mathbf{low})}{2}}{\frac{\mathbf{x}(\mathbf{high}) - \mathbf{x}(\mathbf{low})}{2}}$, $\mathrm{x}: -\boldsymbol{\omega}\ldots, -3, -2, -1, 0, 1, 2, 3, \ldots + \boldsymbol{\omega}$					

had minimum diameter as well as uniform morphology. Fig. 9 shows that at level ***H***, PVA/Cs-CNs had the highest thermal stability (325 °C) and the rate of this stability varied depending on the electrospinning conditions so that sample ***A*** had minimum thermal stability. Values of specific surface area calculated by BET technique are presented in Table 2, according to which samples ***e*** and ***b*** had the maximum and minimum surface areas, respectively. Furthermore, the values of the surface area of the samples synthesized under different conditions of electrospinning method were varied.

3.6. Size distribution (SD)

ANOVA presented in Table 3 can be used to confirm the magnitude of these factors (voltage, spinning distance, flow rate, and PVA concentration) [61]. From Table 3, we note that the main effects were highly significant (all had very small p-value). Moreover, the AB, BC, and AC interactions (p-value < 0.0001, $\alpha = 0.05$) were significant; thus, there was some mild interaction. The electrospinning method, however, provided greater degrees of freedom than any other processes for controlling morphology and size distribution. By increasing the voltage, shorter spinning distance, or decreasing the flow rate, the diameter of nanofibers can be majorly diminished, according to which the terminal jet diameter emerging from the solution was directly proportional to the surface tension and inversely proportional to the total current flowing. Although the solution conductivity increased with the increasing PVA concentration, at the same time, the viscosity of the solution also increased. Since the viscosity and surface tension are directly dependent, increased surface tension would lead to increased terminal jet diameter and, hence, size distribution [62, 63]. Fig. 10 compares the values due to the developed model with those obtained experimentally, notifying acceptable predictability of the model developed for SD optimization.

3.7. Surface area (SA)

The complete ANOVA on SA is summarized in Table 4. Results obtained from this table indicate that the spinning distance and PVA concentration

https://doi.org/10.1016/j.heliyon.2019.e01527

Table 2. Randomized complete 2^{k-1} factorial design for the SD, SA, and TD experiments.

Sample (level)	Std order	Run order	Center Pt	Block	A (kV)	B (cm)	C (mL/h)	D (wt)	REP	SD (nm)	SA (m^2/g)	TS (°C)	Pore diameter (nm)
A	1	1	1	1	−1	−1	−1	−1	1	28.0	1800.3	290.3	1.43
									2	28.1	1800.7	290.1	1.44
B	5	2	1	1	−1	−1	1	1	1	33.4	705.6	312.3	1.59
									2	33.4	700.4	311.5	1.59
C	3	3	1	1	−1	1	−1	1	1	15.4	1730.4	317.7	1.43
									2	15.6	1730.3	317.4	1.43
D	2	4	1	1	1	−1	−1	1	1	17.9	824.5	309.5	1.62
									2	17.8	824.5	308.3	1.63
E	7	5	1	1	−1	1	1	−1	1	10.7	1920.7	321.1	1.81
									2	10.7	192.2	321.0	1.81
F	6	6	1	1	1	−1	1	−1	1	14.3	1840.5	310.7	1.38
									2	14.1	1840.2	310.7	1.39
G	4	7	1	1	1	1	−1	−1	1	24.4	1000.7	319.4	1.55
									2	24.5	1009.2	319.2	1.53
H	8	8	1	1	1	1	1	1	1	22.4	1810.3	325.6	1.49
									2	22.7	1810.6	325.8	1.49

https://doi.org/10.1016/j.heliyon.2019.e01527

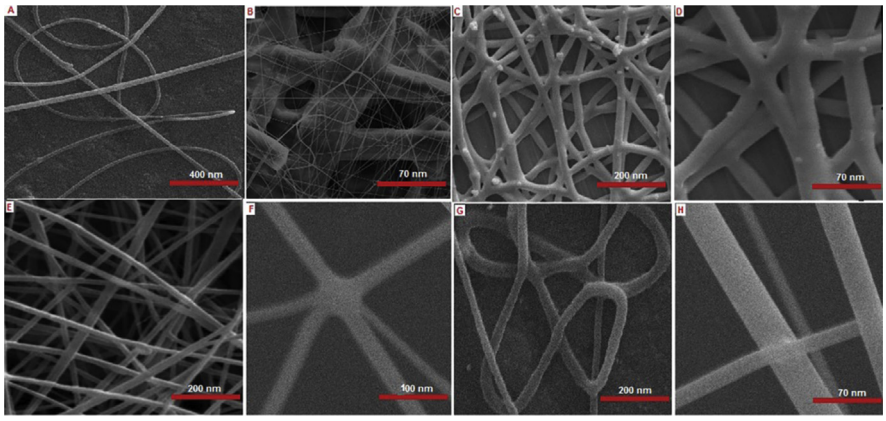

Fig. 8. SEM micrograph of the electrospinning-assisted synthesized PVA/Cs-CNs (A−H).

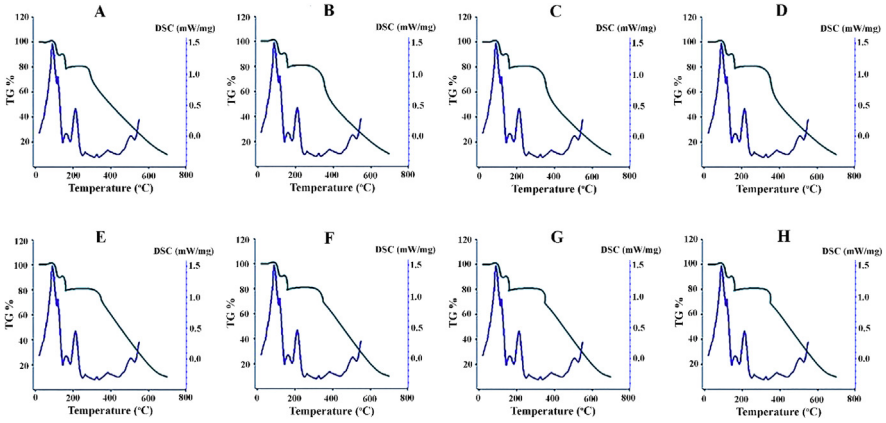

Fig. 9. TGA curves and DSC analysis of the electrospinning-assisted synthesized PVA/Cs-CNs (A−H).

were important factors because all of them had ***p-value*** smaller than α; thus, they would have a significant impact on the surface area of the PVA/Cs-CNs. Also, the AB, BC, and AC interactions (p-value$<$ 0.0001, $\alpha = 0.05$) were significant. Shorter distance between the collector and the tip of the needle applied a reduction in the distance traveled by the jet. Furthermore, there would be an increase in the electric field strength at that time, which increased the acceleration of the jet. Hence, the solvent may not have sufficient time to evaporate, which could result in the incomplete drying. The excess amount of the solvent can also cause the composite fibers to merge where they contact to form junctions and result in inter and intra layer bonding. It should be understand that an enhancement in PVA content would also lead to increased solution conductivity, which would cause greater electrostatic force experienced by the jet eventually lead to increased surface area [64]. Fig. 11 confirms predictability of model developed for SA optimization.

https://doi.org/10.1016/j.heliyon.2019.e01527

Table 3. ANOVA for the SD results.

Source	Sum of squares	df	Mean square	F value	p-Value
Model	820.12	7	117.16	9372.77	<0.0001
A-Voltage	18.49	1	18.49	1479.20	<0.0001
B-Spinning distance	103.02	1	103.02	8241.80	<0.0001
C-Flow rate	6.25	1	6.25	500.00	<0.0001
D-PVA concentration	35.40	1	35.40	2832.20	<0.0001
A*B + C*D	630.01	1	630.01	50400.80	<0.0001
A*C + B*D	9.30	1	9.30	744.20	<0.0001
A*D + B*C	17.64	1	17.64	1411.20	<0.0001
Pure error	0.10	8	0.013		
Core total	820.22	15			
R-Sq: 99.99% R-Sq (pred): 99.95% R-Sq (adj): 99.98%					

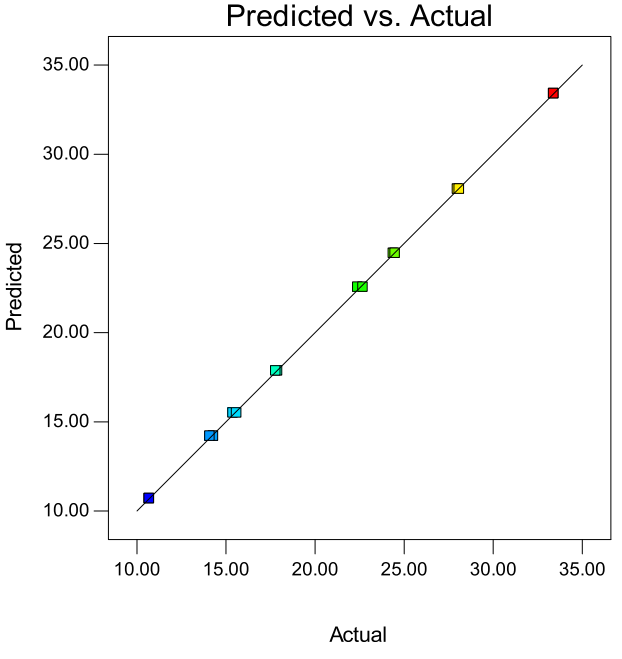

Fig. 10. Predicted values of SD vs. actual values.

3.8. Thermal stability (TS)

ANOVA relating to modeling TS is given in Table 5. We can see that voltage (p-value < 0.0001, $\alpha = 0.05$), spinning distance (p-value < 0.0001, $\alpha = 0.05$), flow rate (p-value < 0.0001, $\alpha = 0.05$), and PVA concentration (p-value < 0.0001, $\alpha = 0.05$) significantly affect the thermal stability of the PVA/Cs-CNs [65]. Effects of the (AB- AC- AD) interactions had p-value less than 0.0001, indicating some

https://doi.org/10.1016/j.heliyon.2019.e01527

Table 4. Analysis of variance for the SA results.

Source	Sum of squares	df	Mean square	F value	p-Value
Model	3.704E+006	7	5.292E+005	84767.37	<0.0001
A-Voltage	1.136E+005	1	1.136E+005	18193.75	<0.0001
B-Spinning distance	4.211E+005	1	4.211E+005	67450.78	<0.0001
C-Flow rate	2.088E+005	1	2.088E+005	33448.98	<0.0001
D-PVA concentration	5.610E+005	1	5.610E+005	89853.01	<0.0001
A*B + C*D	2.484E+005	1	2.484E+005	39784.19	<0.0001
A*C + B*D	1.862E+006	1	1.862E+006	2.982E+005	<0.0001
A*D + B*C	2.901E+005	1	2.901E+005	46469.82	<0.0001
Pure error	49.94	8	6.24		
Core total	3.705E+006	15			
R-Sq: 100% R-Sq (pred): 99.99% R-Sq (adj): 100%					

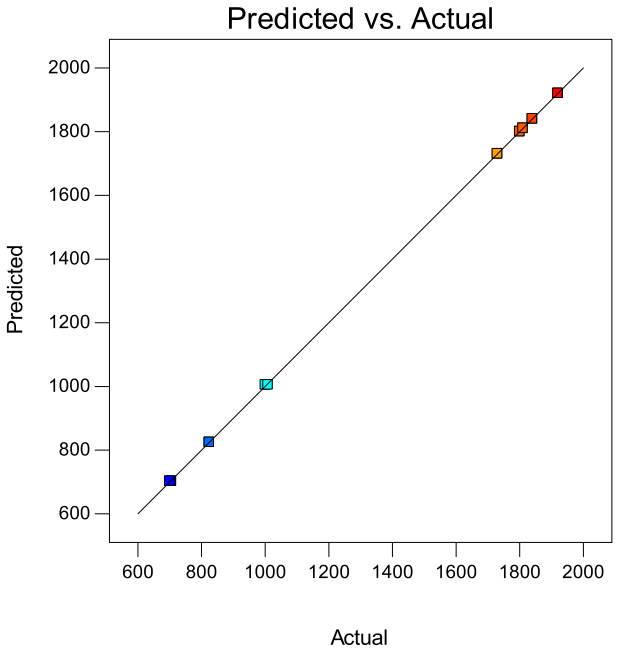

Fig. 11. Predicted values of SA vs. actual values.

interactions between these factors. The increase in thermal stability with the increase of the applied voltage could be due to the dominant effect of the columbic repulsive force. The viscoelastic force increases due to the stretching force exerting on the jet segment with the application of electric field and longitudinal stretching leading to a decrease in the fiber diameter. The change in thermal stability can be due to the fact that the electric field strength decreases as the spinning distance increases, which leads to the decrease in electrostatic forces [66]. The influence of the flow rate on the thermal behaviour can be explained as the density of beads increased on the

https://doi.org/10.1016/j.heliyon.2019.e01527

Table 5. Analysis of variance for the TS results.

Source	Sum of squares	df	Mean square	F value	p-Value
Model	1658.85	7	236.98	1648.54	<0.0001
A-Voltage	142.80	1	142.80	993.41	<0.0001
B-Spinning distance	957.90	1	957.90	6663.67	<0.0001
C-Flow rate	278.89	1	278.89	1940.10	<0.0001
D-PVA concentration	129.96	1	129.96	904.07	<0.0001
A*B + C*D	30.80	1	30.80	214.28	<0.0001
A*C + B*D	72.25	1	72.25	502.61	<0.0001
A*D + B*C	46.24	1	46.24	321.67	<0.0001
Pure error	1.15	8	0.14		
Core total	1660.00	15			
R-Sq: 99.93% R-Sq (pred): 99.72% R-Sq (adj): 99.87%					

fibers. When the flow rate exceeded the critical value, the delivery rate of the solution to the capillary tip exceeded the rate, at which the solution was removed from the tip by the electric forces. This shift in the mass-balance resulted in persistent, but unstable, jet and fibers with more beads were created. Thermal stability with increasing PVA concentration can also be explained in the light of 'electro hydro dynamic (EHD)' theory [67, 68].

According to Fig. 12, the values predicted by the model developed for SA optimization and those of experimental runs are in a very good agreement.

3.9. Process optimization

According to 2^{k-1} factorial design experiments, regression equations in terms of coded factors were:

$$\text{SD (size distribution)} = 20.84 - 1.08A - 2.54B - 0.63C + 1.49D + 6.28AB - 0.76AC - 1.05AD \quad (1)$$

$$\text{SA (surface area)} = 1454.32 - 84.26A + 162.23B + 114.24C - 187.24D - 124.59AB + 341.09AC + 134.66AD \quad (2)$$

$$\text{TS (thermal stability)} = 313.16 + 2.99A + 7.74B + 4.18C + 2.85D - 1.39AB - 2.13AC - 1.70AD \quad (3)$$

Eqs. (1), (2) and (3) are interpolating functions to be used in anticipating properties of PVA/Cs-CNs electrospun nanofibers in terms of input variables. A brighter

https://doi.org/10.1016/j.heliyon.2019.e01527

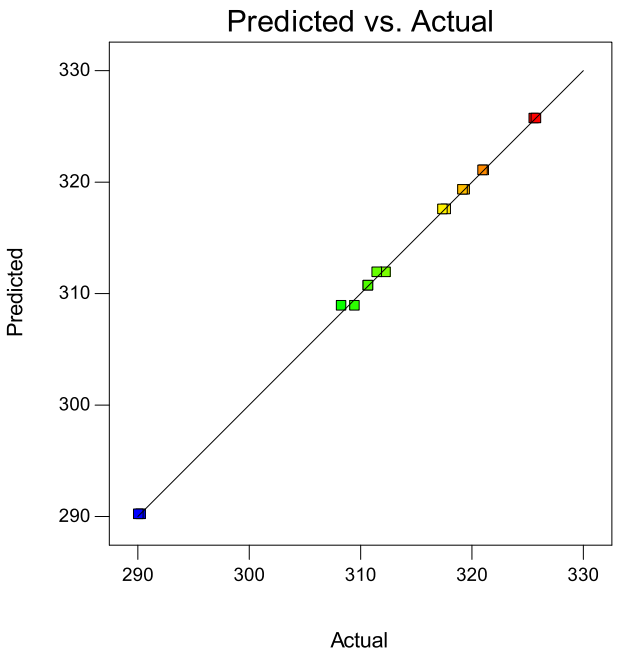

Fig. 12. Predicted values of TS vs. actual values.

prospect of process optimization for deeper understanding the effects of electrospinning requires visual identification of variable effects. Figs. 13, 14, and 15 show the contour plots of SD, SA, and TS obtained from regression models at the current voltage (A), spinning distance (B), flow rate (C), and PVA concentration (D). It is interesting to note that experiments done under similar process conditions (Table 2) were in good agreement with the estimated values. Armed with such outcomes, it is possible to anticipate to an acceptable degree the outcome of process. Not surprisingly, there is no relationship between variations in the SD, SA, and TS. To shed more light on this, it should be noticed that maximum values of SD are obtained at high PVA concentration of 10 wt.% irrespective of flow rate (Fig. 13). By contrast, low PVA concentration of 6 wt.% was responsible for maximization of SA, but again no matter if flow rate is low or high (Fig. 14). On the other hand, a dependency over flow rate was observed in maximization of TS where high concentration of PVA was needed for such goal (Fig. 15). Such findings underline the fact that optimization of PVA/Cs-CNs properties is associated with serious complexities. Fig. 16 shows overlay plots in which the SD, SA and TS responses are requested by the software for taking values in the range of 10−15, 1600−2200 and 315−330, respectively. The plots demonstrate that there is no chance of success at high concentrations of PVA (10 wt.%) to hit the target, while at flow rates of 0.175 mL/h and more likely at 0.2 mL/h when PVA concentration is set to 6 wt.% it would be possible. The desirability value corresponding to the best design with all responses being optimized (minimization of SD and maximization of both SA and TS) are given in Table 6. According to the results obtained by RSM, production of such desired PVA/Cs-CNs

https://doi.org/10.1016/j.heliyon.2019.e01527

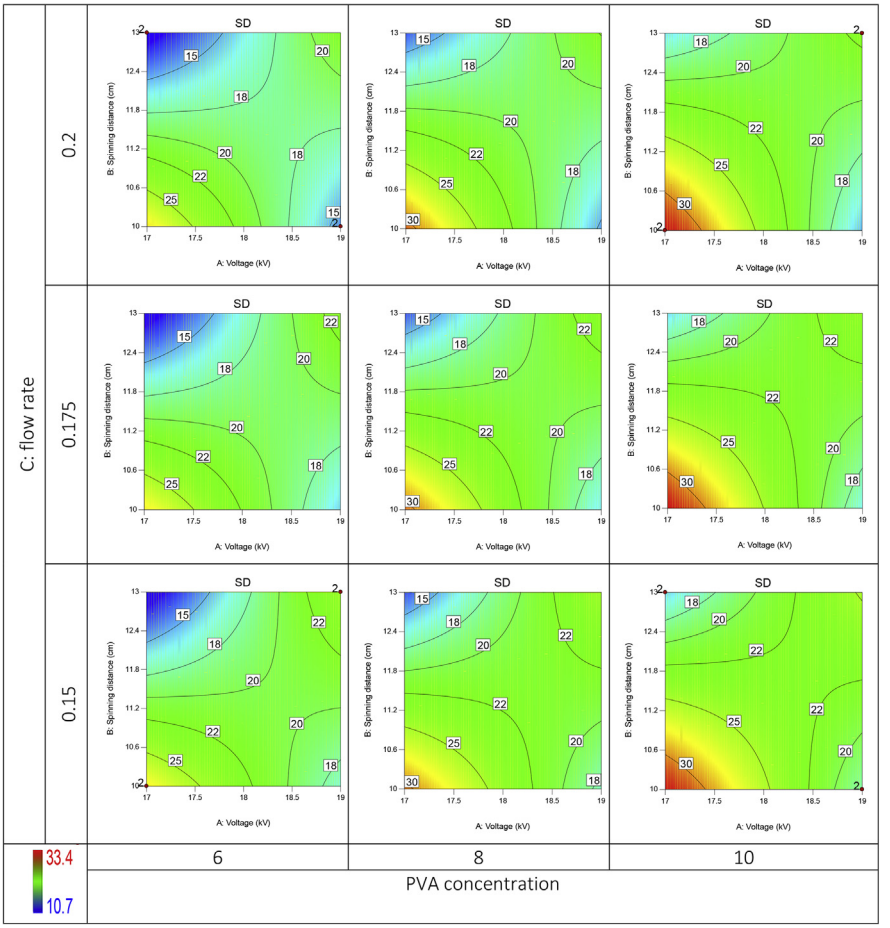

Fig. 13. Contour plots of the size distribution (SD).

electrospun nanofibers is possible with a relatively very high desirability value of 0.953, which suggests adjusting the voltage, spinning distance, flow rate, and PVA concentration at 17 kV, 13 cm, 0.2 mL/h, and 6 wt.%, respectively, to have a product with SD of 10.7 nm, SA of 1920.45 m^2/g, and TS of 321.05 (°C), in the same order as variables. Individual contour plots of desirability with actual values of target outcomes are shown in Fig. 17.

Based on the results obtained from 2^{k-1} factorial design experiments, RSM was practised in use to optimize refolding condition via investigating the influence of the selected variables. In this methodology, the values of the synthesis parameters for the preparation of the PVA/Cs-CNs were predicted through minimizing the size distribution, maximizing the thermal stability, and maximizing the surface area, and their target values were provided as the outputs (Figs. 18, 19, and 20). These properties as well as their predicted values are presented in a non-coded form in Table 7. Attention should be paid to the fact that the formula of converting a code into non-coded form is

https://doi.org/10.1016/j.heliyon.2019.e01527

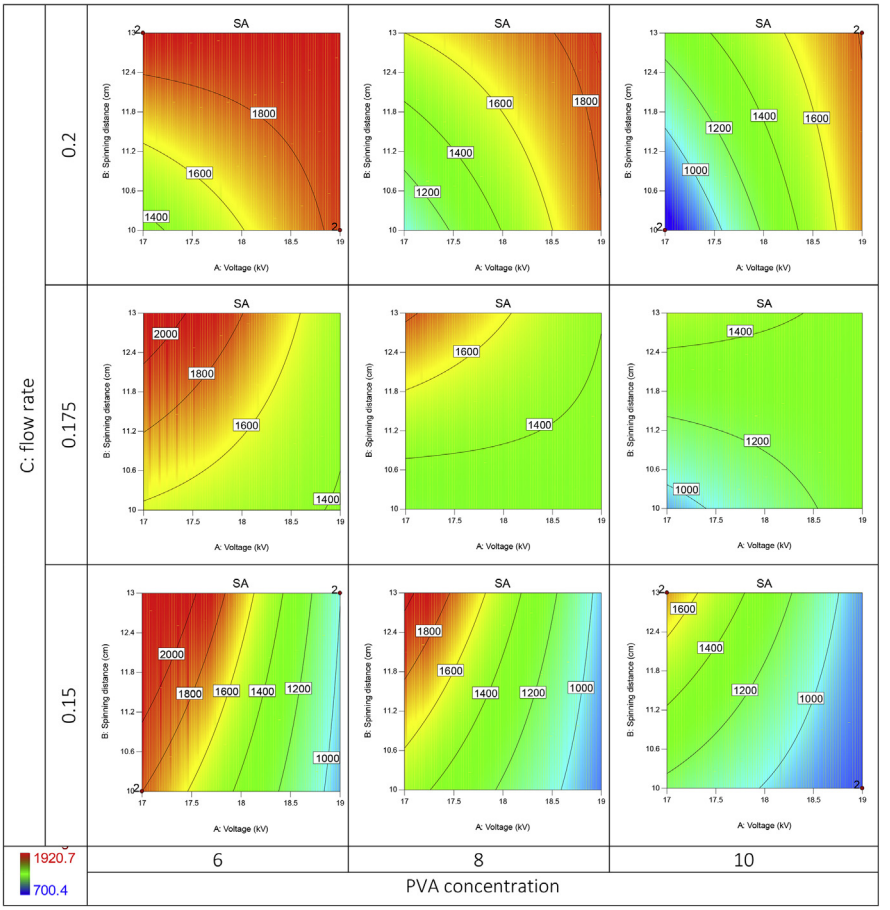

Fig. 14. Contour plots of the surface area (SA).

presented in Table 1. All in all, it has been demonstrated that using such design criteria and armed with factorial design and RSM, a very comprehensive array of response optimization conditions can be achieved to be applied in CO removal in the next stage.

3.10. Superior CO removal efficiency

To study CO adsorption by PVA/Cs-CNs, an adsorptive setup composed of different parts was used, as in Fig. 21.

The procedure was such that, first, a valve was installed between the dozer (storage reservoir) and tank (adsorption reservoir). Consequently, the number of gas moles in the dozer was calculated using Eq. (4):

$$P_1V_1 = Z_1N_1RT \Rightarrow N1 = \frac{P1V1}{Z1RT} \tag{4}$$

https://doi.org/10.1016/j.heliyon.2019.e01527

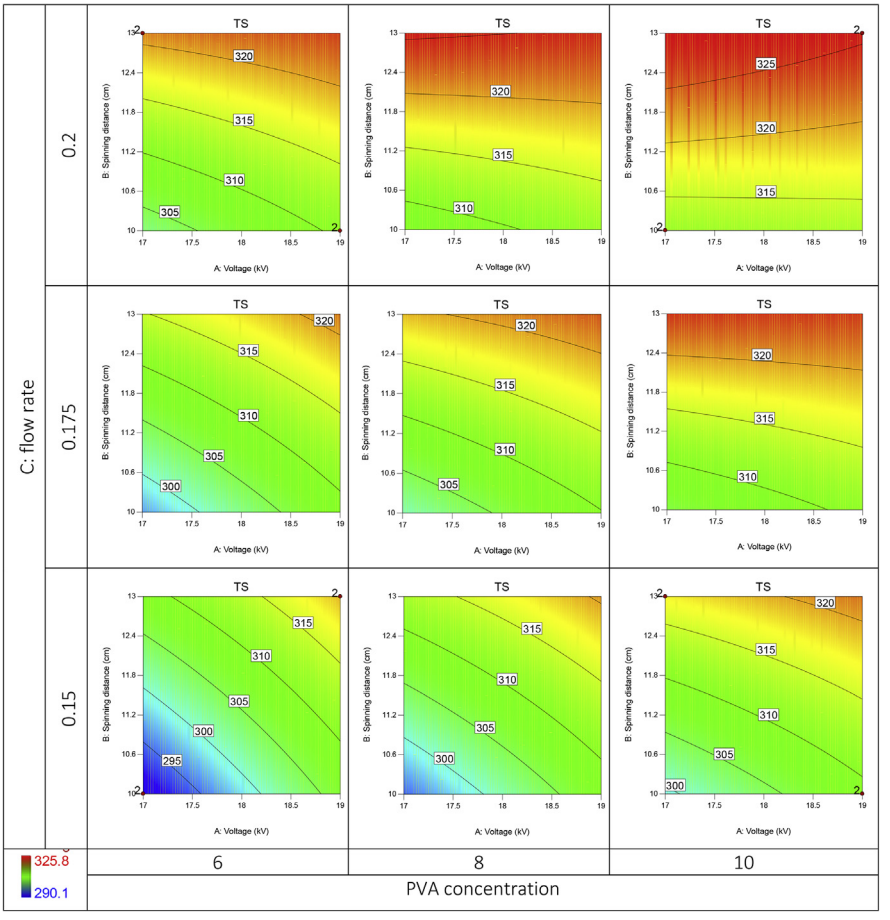

Fig. 15. Surface plots of the thermal stability (TS).

where P_1, N_1, R, T, and Z_1 indicate gas pressure, number of gas moles in the storage reservoir, general constant of gases, equilibrium temperature, and compressibility coefficient in dozer, respectively. At the second stage, the valve between the two reservoirs was opened and the nanofibers were placed inside the tank. As a result of transmission of the gases into the tank, the number of the gas moles in the adsorption reservoir or tank could be calculated by Eq. (5):

$$P_2V_2 = Z_2N_2RT \Rightarrow N2 = \frac{P2V2}{Z2RT} \tag{5}$$

where P_2, Z_2, and V_2 indicate gas pressure, compressibility coefficient factor in the adsorption reservoir, and total volume of the adsorption and storage reservoirs (volume of the nanofiber sample, which is placed in the tank, has been subtracted from the total volume), respectively. Finally, the number of gas moles adsorbed by these composites could be calculated by $n_{ADS} = n_1 - n_2$. The compressibility factor (Z_1, Z_2) was calculated by Eqs. (6), (7), (8), (9), (10) and (11) and Table 8. The values of

https://doi.org/10.1016/j.heliyon.2019.e01527

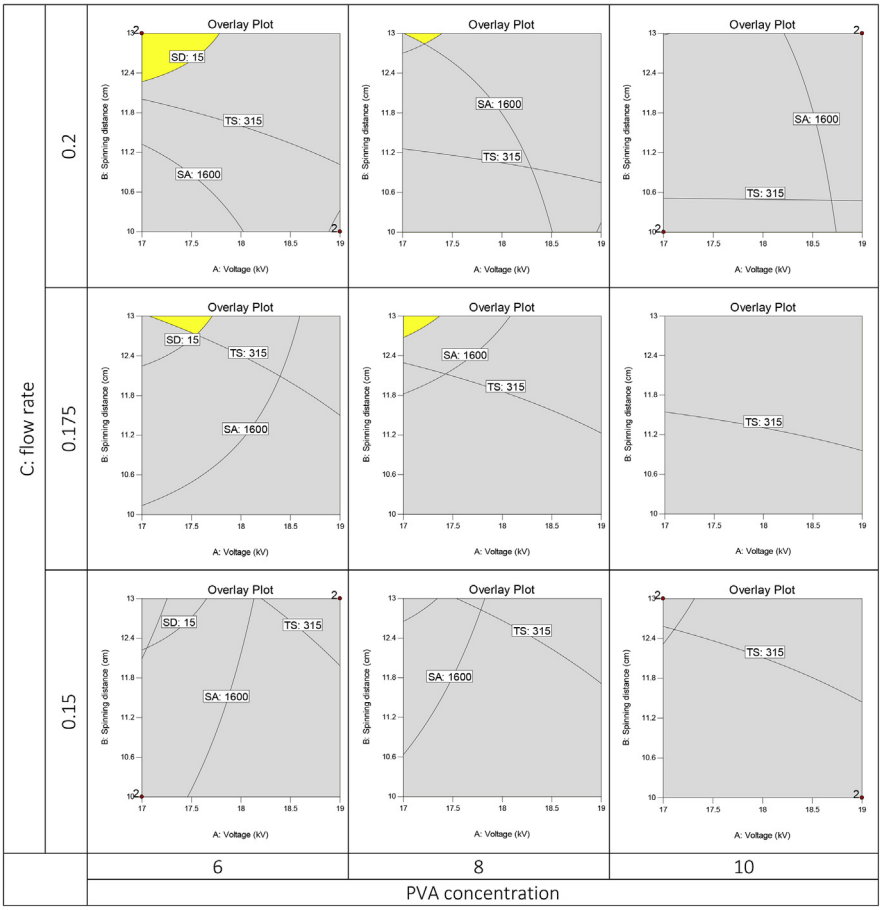

Fig. 16. Overlay plots illustrating optimized regions to maintain the SD, SA and TS in the range of 10−15 nm, 1600−2220 m^2/g and 315−330 °C, respectively.

these coefficients differed depending on the critical temperature and pressure are obtained in this manner [69, 70].

$$z = A + \frac{B + C}{D + E} \tag{6}$$

$$A = aT_r^{2.16} + bp_r^{1.028} + cp_r^{1.58}\, T_r^{-2.1} + d\ln(T_r)^{-0.5} \tag{7}$$

Table 6. Desirability value corresponding to the best set of design variables for optimized production of PVA/Cs-CNs electrospun nanofibers with minimum SD and maximum SA and TS.

Voltage (kV)	Spinning distance (cm)	Flow rate (mL/h)	PVA concentration (wt.%)	SD (nm)	SA (m^2/g)	TS (°C)	Desirability
17.000	13.000	0.200	6.000	10.700	1920.450	321.050	0.953

https://doi.org/10.1016/j.heliyon.2019.e01527

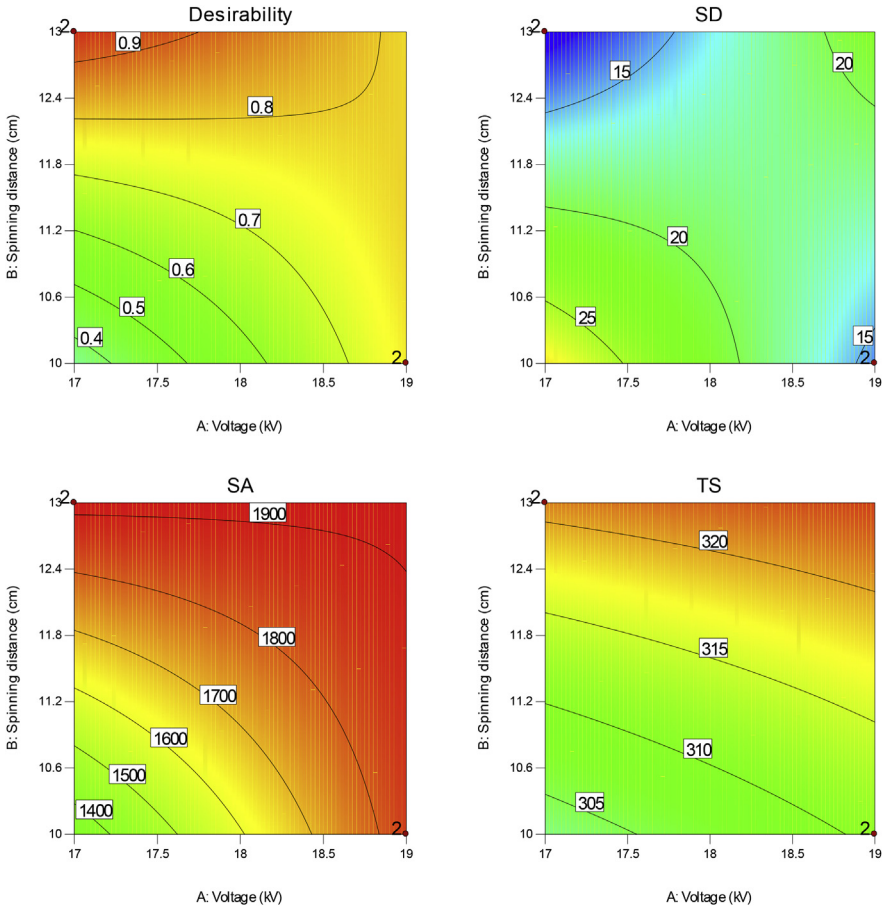

Fig. 17. Contour plots of desirability, SD, SA and TS, for the best case with flow rate of 0.2 mL/h and PVA concentration of 6 wt.%.

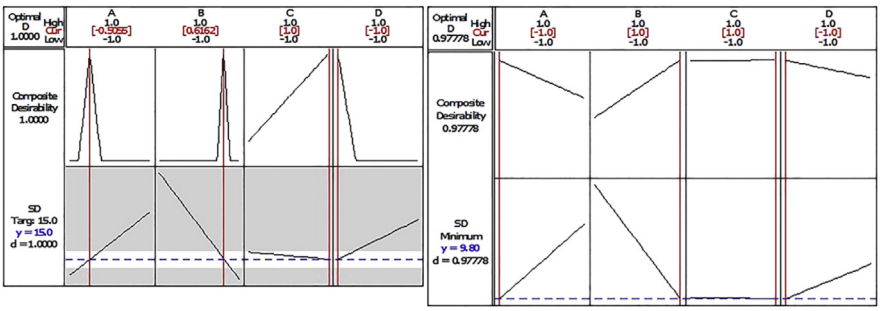

Fig. 18. Optimization plot of the SD using RSM.

$$B = e + fT_r^{2.4} + gp_r^{1.56} + hp_r^{0.125}T_r^{3.033} \tag{8}$$

$$C = i\ln(T_r)^{-1.28} + j\ln(T_r)^{1.37} + k\ln(p_r) + l\ln(p_r)^2 + m\ln(p_r)\ln(T_r) \tag{9}$$

$$D = 1 + nT_r^{5.55} + op_r^{0.68}T_r^{0.33} \tag{10}$$

https://doi.org/10.1016/j.heliyon.2019.e01527

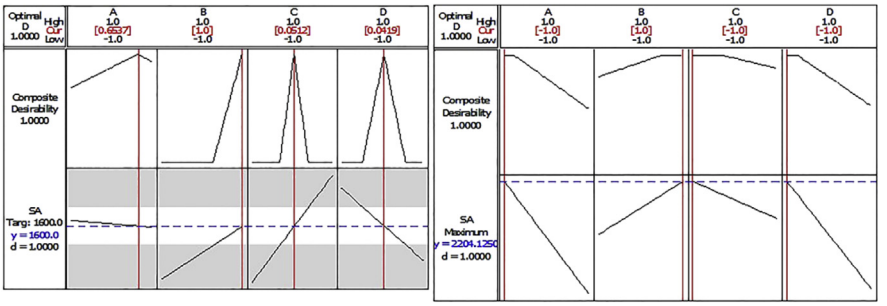

Fig. 19. Optimization plot of the SA using RSM.

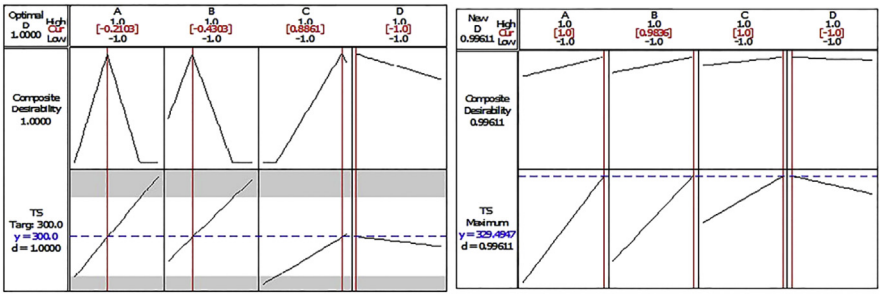

Fig. 20. Optimization plot of the TS using RSM.

$$E = p\ln(T_r)^{1.18} + q\ln(T_r)^{2.1} + r\ln(p_r) + s\ln(p_r)^2 + t\ln(p_r)\ln(T_r) \tag{11}$$

Regarding the RSM optimization results, predicting the parameters of electrospinning method would result in the synthesis of PVA/Cs-CNS with the smallest possible diameter distribution, high surface area, and high thermal stability (results obtained from Table 7). Therefore, after applying the above conditions, the CO gas absorption investigations were performed on the samples. According to Fig. 22, such electrospun fibers exhibited a high CO adsorption rate. Furthermore, the CO adsorption rate was studied in various researches such as metal organic framework [71], zeolite [30] and activated carbon samples [72], and nanofibers have been used as new candidates in recent years. As can be observed, the PVA/Cs-CNs exhibited even higher adsorption potential in comparison. In addition to the application of the synthesis conditions, which leads to the synthesis of products with desirable properties, the use of systematic investigations, which facilitates the synthesis of products with ideal properties, can be considered as one of the distinctions of these composites that results in a higher CO adsorption rate in these composite nanofibers. Table 9 visualizes the superiority of PVA/Cs-CNs synthesized in this work with nanofibers and adsorbents reported in the literature, demonstrating that nanofibrous designed and optimized in this work are completely of a higher class. Since PVA/Cs-CNs are biocompatible and biodegradable and have high adsorption capacity, they can be used as a new platform for the adsorption of various gases.

https://doi.org/10.1016/j.heliyon.2019.e01527

Table 7. Response optimization for the electrospinning parameters (non-coded).

Response	Goal	Lower	Target	Upper	A (kV)	B (cm)	C (mL/h)	D (wt)	Desirability	Predict response value
SD (nm)	Minimize	1	9	45	17.00	13.00	0.20	6.00	0.9778	9.80
	Target	14	15	16	17.49	12.42	0.20	6.00	1.0000	15.00
SA (m^2/gr)	Maximize	500	2100	1500	17.00	13.00	0.15	6.00	1.0000	2204.12
	Target	1500	1600	1700	18.65	10.00	0.17	8.08	1.0000	1600.00
TS (°C)	Maximize	200	330	800	19.00	13.00	0.20	6.00	0.9973	329.65
	Target	290	300	310	17.74	10.85	0.19	6.00	1.0000	300.00

https://doi.org/10.1016/j.heliyon.2019.e01527

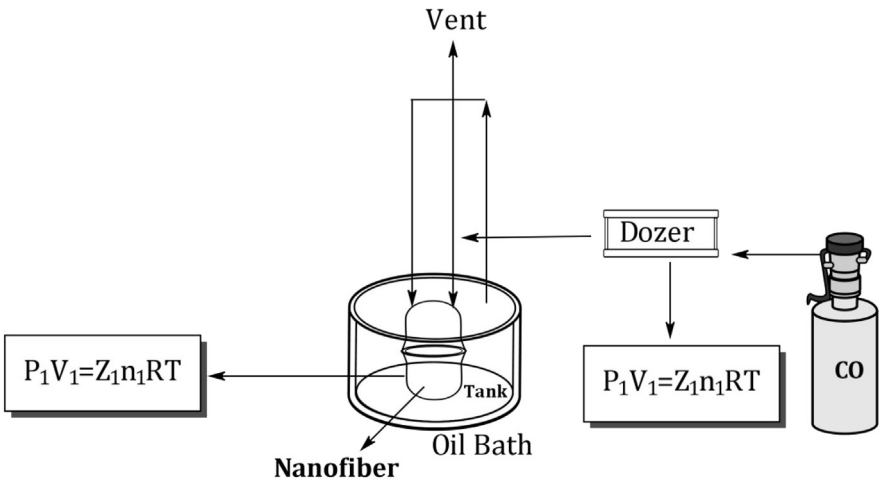

Fig. 21. Different components of adsorption setup for detecting the amount of CO adsorbed in mole.

Although composite nanofibers produced in this study had desired properties providing the conditions for their industrial applications, still their properties as adsorbent can be improved significantly by designing new set of experiments inspired by the lesson learned from multiobjective optimization

Table 8. Values of different coefficients for calculating Z_1 and Z_2.

Coefficients	Values
a	0.0373142485385592
b	−0.0140807151485369
c	0.0163263245387186
d	−0.0307776478819813
e	13843575480.943800
f	−16799138540.763700
g	1624178942.6497600
h	13702270281.086900
i	−41645509.896474600
j	237249967625.01300
k	−24449114791.1531
l	19357955749.3274
m	−126354717916.607
n	623705678.385784
o	17997651104.3330
p	151211393445.064
q	139474437997.172
r	−24233012984.0950
s	18938047327.5205
t	−141401620722.689

https://doi.org/10.1016/j.heliyon.2019.e01527

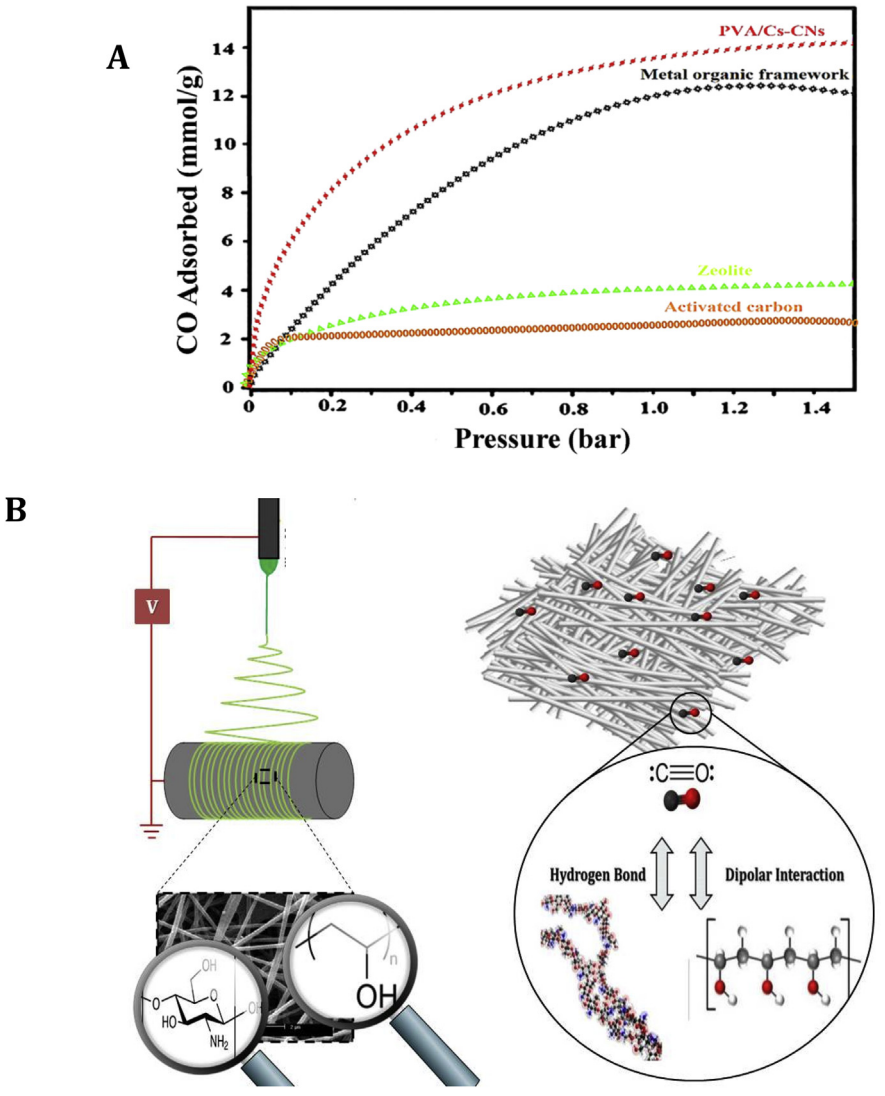

Fig. 22. A) CO adsorption isotherms at 300 K for PVA/Cs-CNs, metal organic framework, zeolite and, activated carbon samples, B) mechanism of the CO adsorption using PVA/Cs-CNs.

performed here. In addition, to enhance the efficiency of these products, they can be produced in composite form with other adsorbent such as zeolites and metal organic framework and to recycle these novel adsorbents developed in this work, magnetic properties can be induced to them that these properties make the collection easier and therefore the longevity of these compounds.

The mechanism of CO adsorption on PVA/Cs can be related to the formation of hydrogen bond and dipolar interaction. Nanostructure of PVA/CS-CNs enhanced the performance of nanofibers in comparison with other adsorbents like activated carbon [73] which is illustrated in Fig. 22A. Adsorption mechanism is also depicted in Fig. 22B. Fiber diameter is the most important factor in gas adsorption. The finer fibers can interact effectively with gas molecules and adsorb the higher amount of the gas.

https://doi.org/10.1016/j.heliyon.2019.e01527

Table 9. Comparing physicochemical properties of PVA/Cs-CNs synthesized in this work with previous cases reported in the literature.

Compound	Thermal stability (°C)	Size distribution (nm)	Surface area (m^2/g)	Ref
PVA/Cs-CNs	**329**	**9.8**	**2204**	**This work**
A novel chitosan functional gel	310	70	9.41	[74]
chitosan based electrospun nanofiber membrane	260	90	13.2	[67]
Chitosan/(polyvinyl alcohol)/zeolite	286	87	47.3	[75]
Ta- metal organic framework	218	73	1940	[50]
PVA/PLZT composite	220	80	-	[65]
PVA/chitosan	290	65	-	[54]
Ni metal organic framework	200	3000	1970	[59]
chitosan/sericin/PVA nanofibers	280	45	-	[56]
Co-metal organic framework	205	3200	2963	[60]

4. Conclusion

Thermally stable chitosan/PVA nanofibers with optimized size distribution and surface area were designed and optimized using electrospinning and revealed a very high level of CO adsorption, even more than what would be expected from the super-adsorbents whose adsorption capacities are reported in the literature. The optimized nanofibers have been identified by the use of factorial design and multiobjective optimization based on RSM and desirability function analyses. In this regard, desired PVA/Cs-CNs electrospun nanofibers having a relatively very high desirability value of 0.953 were obtained by the aid of multiobjective optimization that suggested the best set of electrospinning parameters as voltage, spinning distance, flow rate, and PVA concentration to be set as 17 kV, 13 cm, 0.2 mL/h, and 6 wt.%, respectively. Such optimized conditions led to production of nanofibers with very high thermal stability of 329 °C, very low fiber diameter of 9.8 nm, and surface area of 2204 m^2/g. The optimized sample was applied in CO adsorption, where the amount of CO (14 mmol/g) was much more than the activated carbon and zeolite, and even to some extent higher than metal organic framework. Thanks to its biocompatibility/biodegradability, however, the eco-friendly nanofibrous adsorbents developed and optimized in this work are indeed exclusive. More interestingly, the systematic study performed here based on 2^{k-1} factorial design, RSM and desirability function analyses opens a new era for the optimized synthesis of other nanostructures with desirable properties so as to be applied as super eco-friendly gas absorbents in various fields.

https://doi.org/10.1016/j.heliyon.2019.e01527

Declarations

Author contribution statement

Ghasem Sargazi: Conceived and designed the experiments; Performed the experiments; Analyzed and interpreted the data; Contributed reagents, materials, analysis tools or data.

Daryoush Afzali, Ali Mostafavi: Performed the experiments; Analyzed and interpreted the data; Contributed reagents, materials, analysis tools or data.

Alireza Shadman, Babak Rezaee, Payam Zarrintaj: Analyzed and interpreted the data; Contributed reagents, materials, analysis tools or data.

Mohammad Reza Saeb, Seeram Ramakrishna: Analyzed and interpreted the data; Contributed reagents, materials, analysis tools or data; Wrote the paper.

Masoud Mozafari: Conceived and designed the experiments; Analyzed and interpreted the data.

Funding statement

This research did not receive any specific grant from funding agencies in the public, commercial, or not-for-profit sectors.

Competing interest statement

The authors declare no conflict of interest.

Additional information

No additional information is available for this paper.

References

[1] J.-F. Lutz, J.-M. Lehn, E. Meijer, K. Matyjaszewski, From precision polymers to complex materials and systems, Nat. Rev. Mater. 1 (2016) 16024.

[2] A. Zunger, Inverse design in search of materials with target functionalities, Nat. Rev. Chem. 2 (2018) 0121.

[3] P. Zarrintaj, Z. Ahmadi, M.R. Saeb, M. Mozafari, Poloxamer-based stimuli-responsive biomaterials, Mater. Today Proc. 5 (2018) 15516−15523.

[4] H.R. Ebrahimi Jahromi, G.R. Bakhshandeh, A. Ebrahimi Jahromi, M.R. Saeb, Z. Ahmadi, A.S. Pakdel, A comparative study to assess structure−properties

https://doi.org/10.1016/j.heliyon.2019.e01527

relationships in (acrylonitrile butadiene rubber)-based composites: recycled microfillers versus nanofillers, J. Vinyl Addit. Technol. 23 (2017) 13−20.

[5] H. Rastin, Z. Ahmadi, A.S. Pakdel, M.R. Saeb, Y. Abbasian, M. Liravi, A. Eslahi, A physicochemical route for compensation of molecular weight loss during recycling of poly (ethylene terephthalate), J. Vinyl Addit. Technol. 22 (2016) 387−395.

[6] P. Zarrintaj, B. Bakhshandeh, M.R. Saeb, F. Sefat, I. Rezaeian, M.R. Ganjali, S. Ramakrishna, M. Mozafari, Oligoaniline-based conductive biomaterials for tissue engineering, Acta Biomater. (2018).

[7] P. Zarrintaj, B. Bakhshandeh, I. Rezaeian, B. Heshmatian, M.R. Ganjali, A novel electroactive agarose-aniline pentamer platform as a potential candidate for neural tissue engineering, Sci. Rep. 7 (2017) 17187.

[8] P. Zarrintaj, A. Urbanska, S.S. Gholizadeh, V. Goodarzi, M.R. Saeb, M. Mozafari, A facile route to the synthesis of anilinic electroactive colloidal hydrogels for neural tissue engineering applications, J. Colloid Interface Sci. (2018).

[9] Z. Atoufi, P. Zarrintaj, G.H. Motlagh, A. Amiri, Z. Bagher, S.K. Kamrava, A novel bio electro active alginate-aniline tetramer/agarose scaffold for tissue engineering: synthesis, characterization, drug release and cell culture study, J. Biomater. Sci. Polym. Ed. 28 (2017) 1617−1638.

[10] P. Zarrintaj, S. Manouchehri, Z. Ahmadi, M.R. Saeb, A.M. Urbanska, D.L. Kaplan, M. Mozafari, Agarose-based biomaterials for tissue engineering, Carbohydr. Polym. (2018).

[11] M. Rahmati, P.B. Milan, A. Samadikuchaksaraei, V. Goodarzi, M.R. Saeb, S. Kargozar, D.L. Kaplan, M. Mozafari, Ionically crosslinked thermoresponsive chitosan hydrogels formed in situ: a conceptual basis for deeper understanding, Macromol. Mater. Eng. (2017) 302.

[12] S. Manouchehri, B. Bagheri, S.H. Rad, M.N. Nezhad, Y.C. Kim, O.O. Park, M. Farokhi, M. Jouyandeh, M.R. Ganjali, M.K. Yazdi, Electroactive bio-epoxy incorporated chitosan-oligoaniline as an advanced hydrogel coating for neural interfaces, Prog. Org. Coatings 131 (2019) 389−396.

[13] Z. Bagher, Z. Atoufi, R. Alizadeh, M. Farhadi, P. Zarrintaj, L. Moroni, M. Setayeshmehr, A. Komeili, S.K. Kamrava, Conductive hydrogel based on chitosan-aniline pentamer/gelatin/agarose significantly promoted motor neuron-like cells differentiation of human olfactory ecto-mesenchymal stem cells, Mater. Sci. Eng. C (2019).

https://doi.org/10.1016/j.heliyon.2019.e01527

[14] S.A. Poursamar, M. Azami, M. Mozafari, Controllable synthesis and characterization of porous polyvinyl alcohol/hydroxyapatite nanocomposite scaffolds via an in situ colloidal technique, Colloids Surf. B Biointerfaces 84 (2011) 310–316.

[15] S.N. Alhosseini, F. Moztarzadeh, M. Mozafari, S. Asgari, M. Dodel, A. Samadikuchaksaraei, S. Kargozar, N. Jalali, Synthesis and characterization of electrospun polyvinyl alcohol nanofibrous scaffolds modified by blending with chitosan for neural tissue engineering, Int. J. Nanomed. 7 (2012) 25.

[16] M.A. Shokrgozar, F. Mottaghitalab, V. Mottaghitalab, M. Farokhi, Fabrication of porous chitosan/poly (vinyl alcohol) reinforced single-walled carbon nanotube nanocomposites for neural tissue engineering, J. Biomed. Nanotechnol. 7 (2011) 276–284.

[17] M.R. Saeb, Y. Mohammadi, T.S. Kermaniyan, P. Zinck, F.J. Stadler, Unspoken aspects of chain shuttling reactions: patterning the molecular landscape of olefin multi-block copolymers, Polymer 116 (2017) 55–75.

[18] F. Mottaghitalab, M. Farokhi, V. Mottaghitalab, M. Ziabari, A. Divsalar, M.A. Shokrgozar, Enhancement of neural cell lines proliferation using nano-structured chitosan/poly (vinyl alcohol) scaffolds conjugated with nerve growth factor, Carbohydr. Polym. 86 (2011) 526–535.

[19] M. Koosha, H. Mirzadeh, M.A. Shokrgozar, M. Farokhi, Nanoclay-reinforced electrospun chitosan/PVA nanocomposite nanofibers for biomedical applications, RSC Adv. 5 (2015) 10479–10487.

[20] P. Wang, H. Wang, J. Liu, P. Wang, S. Jiang, X. Li, S. Jiang, Montmorillonite@ chitosan-poly (ethylene oxide) nanofibrous membrane enhancing poly (vinyl alcohol-co-ethylene) composite film, Carbohydr. Polym. 181 (2018) 885–892.

[21] P. Zarrintaj, A.S. Moghaddam, S. Manouchehri, Z. Atoufi, A. Amiri, M.A. Amirkhani, M.A. Nilforoushzadeh, M.R. Saeb, M.R. Hamblin, M. Mozafari, Can regenerative medicine and nanotechnology combine to heal wounds? The search for the ideal wound dressing, Nanomedicine 12 (2017) 2403–2422.

[22] Y. Zhou, C. Zhang, K. Liang, J. Li, H. Yang, X. Liu, X. Yin, D. Chen, W. Xu, Photopolymerized water-soluble maleilated chitosan/methacrylated poly (vinyl alcohol) hydrogels as potential tissue engineering scaffolds, Int. J. Biol. Macromol. 106 (2018) 227–233.

[23] Y. Zhou, S. Zhao, C. Zhang, K. Liang, J. Li, H. Yang, S. Gu, Z. Bai, D. Ye, W. Xu, Photopolymerized maleilated chitosan/thiol-terminated poly (vinyl

 https://doi.org/10.1016/j.heliyon.2019.e01527

alcohol) hydrogels as potential tissue engineering scaffolds, Carbohydr. Polym. (2018).

[24] S. Kumar, B. Krishnakumar, A.J. Sobral, J. Koh, Bio-based (chitosan/PVA/ZnO) nanocomposites film: thermally stable and photoluminescence material for removal of organic dye, Carbohydr. Polym. 205 (2019) 559−564.

[25] S. Koushkbaghi, A. Zakialamdari, M. Pishnamazi, H.F. Ramandi, M. Aliabadi, M. Irani, Aminated-Fe_3O_4 nanoparticles filled chitosan/PVA/PES dual layers nanofibrous membrane for the removal of Cr (VI) and Pb (II) ions from aqueous solutions in adsorption and membrane processes, Chem. Eng. J. 337 (2018) 169−182.

[26] M.R. Karim, M.O. Aijaz, N.H. Alharth, H.F. Alharbi, F.S. Al-Mubaddel, M.R. Awual, Composite nanofibers membranes of poly (vinyl alcohol)/chitosan for selective lead (II) and cadmium (II) ions removal from wastewater, Ecotoxicol. Environ. Saf. 169 (2019) 479−486.

[27] L.D. Prockop, R.I. Chichkova, Carbon monoxide intoxication: an updated review, J. Neurol. Sci. 262 (2007) 122−130.

[28] W. Yan, Carbon monoxide, the silent killer, may have met its match, in: American Association for the Advancement of Science, 2016.

[29] K. Sircar, J. Clower, M. kyong Shin, C. Bailey, M. King, F. Yip, Carbon monoxide poisoning deaths in the United States, 1999 to 2012, Am. J. Emerg. Med. 33 (2015) 1140−1145.

[30] Y. Park, Y. Ju, D. Park, C.-H. Lee, Adsorption equilibria and kinetics of six pure gases on pelletized zeolite 13X up to 1.0 MPa: CO_2, CO, N_2, CH_4, Ar and H_2, Chem. Eng. J. 292 (2016) 348−365.

[31] K. Chakarova, S. Andonova, L. Dimitrov, K. Hadjiivanov, FTIR study of CO and N_2 adsorption on [Ge] FAU zeolites in their Na-and H-forms, Microporous Mesoporous Mater. 220 (2016) 188−197.

[32] M. Servatan, M. Ghadiri, A.T. Damanabi, F. Bahadori, P. Zarrintaj, Z. Ahmadi, H. Vahabi, M.R. Saeb, Zeolite-based catalysts for exergy efficiency enhancement: the insights gained from nanotechnology, Mater. Today Proc. 5 (2018) 15868−15876.

[33] M.R. Derakhshandeh, M.J. Eshraghi, M.M. Hadavi, M. Javaheri, S. Khamseh, M.G. Sari, P. Zarrintaj, M.R. Saeb, M. Mozafari, Diamond-like carbon thin films prepared by pulsed-DC PE-CVD for biomedical applications, Surf. Innov. 6 (2018) 167−175.

https://doi.org/10.1016/j.heliyon.2019.e01527

[34] V. Beachley, X. Wen, Polymer nanofibrous structures: fabrication, biofunctionalization, and cell interactions, Prog. Polym. Sci. 35 (2010) 868−892.

[35] H. Ghasemi Hamidabadi, Z. Rezvani, M. Nazm Bojnordi, H. Shirinzadeh, A.M. Seifalian, M.T. Joghataei, M. Razaghpour, A. Alibakhshi, A. Yazdanpanah, M. Salimi, Chitosan-intercalated montmorillonite/poly (vinyl alcohol) nanofibers as a platform to guide neuronlike differentiation of human dental pulp stem cells, ACS Appl. Mater. Interfaces 9 (2017) 11392−11404.

[36] Z. Rezvani, J.R. Venugopal, A.M. Urbanska, D.K. Mills, S. Ramakrishna, M. Mozafari, A bird's eye view on the use of electrospun nanofibrous scaffolds for bone tissue engineering: current state-of-the-art, emerging directions and future trends, Nanomed. Nanotechnol. Biol. Med. 12 (2016) 2181−2200.

[37] X. Zhou, H. Yi, X. Tang, H. Deng, H. Liu, Thermodynamics for the adsorption of SO_2, NO and CO_2 from flue gas on activated carbon fiber, Chem. Eng. J. 200 (2012) 399−404.

[38] S. Luo, S. Chen, Y. Chen, S. Chen, N. Ma, Q. Wu, Sisal fiber-based solid amine adsorbent and its kinetic adsorption behaviors for CO_2, RSC Adv. 6 (2016) 72022−72029.

[39] Y. Mohammadi, M.R. Saeb, A. Penlidis, E. Jabbari, P. Zinck, F.J. Stadler, K. Matyjaszewski, Intelligent Monte Carlo: a new paradigm for inverse polymerization engineering, Macromol. Theory Simul. (2018) 1700106.

[40] M.R. Saeb, Y. Mohammadi, A.S. Pakdel, A. Penlidis, Molecular architecture manipulation in free radical copolymerization: an advanced Monte Carlo approach to screening copolymer chains with various comonomer sequence arrangements, Macromol. Theory Simul. 25 (2016) 369−382.

[41] M.R. Saeb, Y. Mohammadi, M. Ahmadi, M.M. Khorasani, F.J. Stadler, A Monte Carlo-based feeding policy for tailoring microstructure of copolymer chains: reconsidering the conventional metallocene catalyzed polymerization of α-olefins, Chem. Eng. J. 274 (2015) 169−180.

[42] M.R. Saeb, M.M. Khorasani, M. Ahmadi, Y. Mohammadi, F.J. Stadler, A unified picture of hard-soft segmental development along olefin chain shuttling copolymerization, Polymer 76 (2015) 245−253.

[43] B. Shirkavand Hadavand, M.R. Saeb, F. Najafi, A. Malekian, Response surface analysis for understanding the effects of synthesis parameters on the microstructure of hyperbranched polyesters, J. Macromol. Sci. Part A 53 (2016) 741−749.

https://doi.org/10.1016/j.heliyon.2019.e01527

[44] M. Saeb, M. Moghri, Application of response surface methodology in describing fusion characteristics of rigid poly (vinyl chloride)/nanoclay/wood flour/calcium carbonate hybrid nanocomposites, J. Vinyl Addit. Technol. 21 (2015) 183−190.

[45] G. Mahmodi, S. Sharifnia, F. Rahimpour, S. Hosseini, Photocatalytic conversion of CO_2 and CH_4 using ZnO coated mesh: effect of operational parameters and optimization, Sol. Energy Mater. Sol. Cells 111 (2013) 31−40.

[46] F. Andami, M. Ataeefard, F. Najafi, M.R. Saeb, Understanding the interactive effects of material parameters governing the printer toner properties: a response surface study, J. Polym. Eng. 37 (2017) 587−597.

[47] A.S. Pakdel, M. Rezaei Behbahani, M.R. Saeb, H.A. Khonakdar, H. Abedini, M. Moghri, Evolution of vinyl chloride conversion below critical micelle concentration: a response surface analysis, J. Vinyl Addit. Technol. 21 (2015) 157−165.

[48] S. Mohebbi, M.N. Nezhad, P. Zarrintaj, S.H. Jafari, S.S. Gholizadeh, M.R. Saeb, M. Mozafari, Chitosan in biomedical engineering: a critical review, Curr. Stem Cell Res. Ther. (2018).

[49] L.-L. Min, L.-M. Yang, R.-X. Wu, L.-B. Zhong, Z.-H. Yuan, Y.-M. Zheng, Enhanced adsorption of arsenite from aqueous solution by an iron-doped electrospun chitosan nanofiber mat: preparation, characterization and performance, J. Colloid Interface Sci. 535 (2019) 255−264.

[50] G. Sargazi, D. Afzali, A. Mostafavi, S.Y. Ebrahimipour, Ultrasound-assisted facile synthesis of a new tantalum (V) metal-organic framework nanostructure: design, characterization, systematic study, and CO_2 adsorption performance, J. Solid State Chem. 250 (2017) 32−48.

[51] J. Lu, Covariate adjustment in randomization-based causal inference for 2K factorial designs, Stat. Probab. Lett. 119 (2016) 11−20.

[52] H. Kashudhan, A. Dixit, A. Upadhyay, Optimization of ingredients for the development of wheatgrass based therapeutical juice using response surface methodology (RSM), J. Pharmacogn. Phytochem. 6 (2017) 338−345.

[53] A. Asfaram, M. Ghaedi, E. Alipanahpour, S. Agarwal, V.K. Gupta, Application of response surface methodology and dispersive liquid−liquid microextraction by microvolume spectrophotometry method for rapid determination of curcumin in water, wastewater, and food samples, Food Anal. Methods 9 (2016) 1274−1283.

https://doi.org/10.1016/j.heliyon.2019.e01527

[54] C. Santos, C.J. Silva, Z. Büttel, R. Guimarães, S.B. Pereira, P. Tamagnini, A. Zille, Preparation and characterization of polysaccharides/PVA blend nanofibrous membranes by electrospinning method, Carbohydr. Polym. 99 (2014) 584−592.

[55] Y. Boonsongrit, B.W. Mueller, A. Mitrevej, Characterization of drug−chitosan interaction by 1 H NMR, FTIR and isothermal titration calorimetry, Eur. J. Pharm. Biopharm. 69 (2008) 388−395.

[56] E. Hadipour-Goudarzi, M. Montazer, M. Latifi, A.A.G. Aghaji, Electrospinning of chitosan/sericin/PVA nanofibers incorporated with in situ synthesis of nano silver, Carbohydr. Polym. 113 (2014) 231−239.

[57] T.C. Wang, W. Bury, D.A. Gómez-Gualdrón, N.A. Vermeulen, J.E. Mondloch, P. Deria, K. Zhang, P.Z. Moghadam, A.A. Sarjeant, R.Q. Snurr, Ultrahigh surface area zirconium MOFs and insights into the applicability of the BET theory, J. Am. Chem. Soc. 137 (2015) 3585−3591.

[58] R. Mincheva, N. Manolova, R. Sabov, G. Kjurkchiev, I. Rashkov, Hydrogels from chitosan crosslinked with poly (ethylene glycol) diacid as bone regeneration materials, e-Polymers 4 (2004) 643−653.

[59] G. Sargazi, D. Afzali, N. Daldosso, H. Kazemian, N. Chauhan, Z. Sadeghian, T. Tajerian, A. Ghafarinazari, M. Mozafari, A systematic study on the use of ultrasound energy for the synthesis of nickel−metal organic framework compounds, Ultrason. Sonochem. 27 (2015) 395−402.

[60] G. Sargazi, D. Afzali, A. Ghafainazari, H. Saravani, Rapid synthesis of cobalt metal organic framework, J. Inorg. Organomet. Polym. Mater. 24 (2014) 786−790.

[61] A. Rogina, Electrospinning process: versatile preparation method for biodegradable and natural polymers and biocomposite systems applied in tissue engineering and drug delivery, Appl. Surf. Sci. 296 (2014) 221−230.

[62] L. Wannatong, A. Sirivat, P. Supaphol, Effects of solvents on electrospun polymeric fibers: preliminary study on polystyrene, Polym. Int. 53 (2004) 1851−1859.

[63] A. Khalil, R. Hashaikeh, M. Jouiad, Synthesis and morphology analysis of electrospun copper nanowires, J. Mater. Sci. 49 (2014) 3052−3065.

[64] I.D. Kim, A. Rothschild, Nanostructured metal oxide gas sensors prepared by electrospinning, Polym. Adv. Technol. 22 (2011) 318−325.

https://doi.org/10.1016/j.heliyon.2019.e01527

[65] S. Singh, S. Roy, V. Singh, M. Vijayakumar, Synthesis and morphology of electrospun PVA/PLZT composite and single phase PLZT nanofibers, Mater. Sci. Eng. B 176 (2011) 1099−1109.

[66] Y. Ahn, S. Park, G. Kim, Y. Hwang, C. Lee, H. Shin, J. Lee, Development of high efficiency nanofilters made of nanofibers, Curr. Appl. Phys. 6 (2006) 1030−1035.

[67] L.-L. Min, Z.-H. Yuan, L.-B. Zhong, Q. Liu, R.-X. Wu, Y.-M. Zheng, Preparation of chitosan based electrospun nanofiber membrane and its adsorptive removal of arsenate from aqueous solution, Chem. Eng. J. 267 (2015) 132−141.

[68] C. Mit-uppatham, M. Nithitanakul, P. Supaphol, Ultrafine electrospun polyamide-6 fibers: effect of solution conditions on morphology and average fiber diameter, Macromol. Chem. Phys. 205 (2004) 2327−2338.

[69] M. Mahmoud, Development of a new correlation of gas compressibility factor (Z-factor) for high pressure gas reservoirs, J. Energy Resour. Technol. 136 (2014) 012903.

[70] A. Kamari, A. Hemmati-Sarapardeh, S.-M. Mirabbasi, M. Nikookar, A.H. Mohammadi, Prediction of sour gas compressibility factor using an intelligent approach, Fuel Process. Technol. 116 (2013) 209−216.

[71] A.-R. Kim, T.-U. Yoon, S.-I. Kim, K. Cho, S.-S. Han, Y.-S. Bae, Creating high CO/CO_2 selectivity and large CO working capacity through facile loading of Cu (I) species into an iron-based mesoporous metal-organic framework, Chem. Eng. J. 348 (2018) 135−142.

[72] M. Aprianti, P. Sheilla, I. Machdar, Optimization process of carbon Mono oxide (CO) gas emission adsorption using activated carbon from rice husk, in: Journal of Physics: Conference Series, IOP Publishing, 2018, p. 012014.

[73] M.M. Ayad, N.A. Salahuddin, I.M. Minisy, W.A. Amer, Chitosan/polyaniline nanofibers coating on the quartz crystal microbalance electrode for gas sensing, Sensor. Actuators B Chem. 202 (2014) 144−153.

[74] M.K. Kim, K.S. Sundaram, G.A. Iyengar, K.-P. Lee, A novel chitosan functional gel included with multiwall carbon nanotube and substituted polyaniline as adsorbent for efficient removal of chromium ion, Chem. Eng. J. 267 (2015) 51−64.

[75] U. Habiba, A.M. Afifi, A. Salleh, B.C. Ang, Chitosan/(polyvinyl alcohol)/zeolite electrospun composite nanofibrous membrane for adsorption of Cr 6+, Fe 3+ and Ni 2+, J. Hazard. Mater. 322 (2017) 182−194.

https://doi.org/10.1016/j.heliyon.2019.e01527